Structure and properties of totally synthetic galacto- and gluco-cerebrosides

Kumkum Saxena,[1,*] Richard I. Duclos,[*] Peter Zimmermann,[†] Richard R. Schmidt,[†] and G. Graham Shipley[2,*]

Departments of Biophysics and Biochemistry,* Center for Advanced Biomedical Research, Boston University School of Medicine, 80 East Concord Street, Boston, MA 02118-2394, and Fakultat Chemie,[†] Universitat Konstanz, D-7750 Konstanz, Germany

Abstract **The structural and thermal properties of aqueous dispersions of the totally synthetic cerebrosides, D-erythro-N-palmitoyl galactosyl- and glucosyl-C_{18}-sphingosine (C16:0-GalCer and C16:0-GluCer, respectively) have been studied using differential scanning calorimetry (DSC) and X-ray diffraction. Over the temperature range 0–100°C, both C16:0-GalCer and C16:0-GluCer show complex thermal transitions characteristic of polymorphic behavior of exclusively bilayer phases. On heating, hydrated C16:0-GalCer undergoes an exothermic bilayer–bilayer transition at 59°C to produce a stable bilayer crystal form. X-ray diffraction at 70°C reveals a bilayer structure with an ordered hydrocarbon chain-packing arrangement. This ordered bilayer phase undergoes an endothermic chain-melting transition at 85°C to the bilayer liquid crystalline state. Similar behavior is exhibited by hydrated C16:0-GluCer which undergoes the exothermic transition at 49°C and a chain-melting transition at 87°C. The exothermic transitions observed on heating hydrated C16:0-GalCer and C16:0-GluCer are irreversible and dependent upon previous chain melting, prior cooling rate, and time of incubation at low temperatures. Thus, the structure and properties of totally synthetic C16:0-GalCer and C16:0-GluCer with identical sphingosine (C18:1) and fatty acid (C16:0) chains are quite similar, suggesting that the precise isomeric structure of the linked sugar plays only a minor role in regulating the properties of hydrated cerebrosides. Further, these studies indicate that the complex thermal behavior and bilayer phase formation exhibited by these single-sugar cerebrosides are intrinsic properties and not due to the heterogeneity of the sphingosine base found in natural and partially synthetic cerebrosides.**—Saxena, K., R. I. Duclos, P. Zimmermann, R. R. Schmidt, and G. G. Shipley. **Structure and properties of totally synthetic galacto- and gluco-cerebrosides.** ***J. Lipid Res.*** **1999.** 40: **839–849.**

Supplementary key words differential scanning calorimetry • X-ray diffraction • lipid bilayers • hydrocarbon chain packing • hydrogen bonding • glycolipids

Glycosphingolipids, GSL, are complex lipids with a lipophilic component (ceramide composed of a long-chain fatty acid amide-linked to a long-chain base, usually sphingosine) and a hydrophilic sugar moiety attached via an ether linkage to sphingosine. GSL are found in relatively large amounts in the myelin sheath of central and peripheral nervous system. Glycosphingolipids can also act as cell surface receptors for hormones, bacterial toxins and viruses (1–3).

We have been interested in defining the structure and properties of GSL of increasing oligosaccharide complexity with a view to understanding both their structural role in membranes and their functional role as receptors; an example of the latter would include our studies of the ganglioside G_{M1}-cholera toxin complex (4–7). In this paper, we focus on the properties of two "simple" monoglycosyl GSL, galacto- and gluco-cerebroside, GalCer and GluCer, respectively.

The physical properties of both natural and partially synthetic cerebrosides have been studied by X-ray diffraction, differential scanning calorimetry (DSC), and spectroscopic methods. For example, early X-ray diffraction studies showed that bovine brain cerebrosides containing predominantly long chain fatty acids (C24:0, C24:1, and C18:0) undergo a chain-melting transition at a relatively high temperature (8). Using DSC, Curatolo (9) studied two subfractions of bovine brain cerebrosides, those containing amide-linked 2-hydroxy fatty acids and amide-linked nonhydroxylated fatty acids (HFA-CER and NFA-CER, respectively). NFA-CER exhibits two low temperature phases, a metastable phase converting exothermically to a stable phase at ~50°C (ΔH = 16–17 cal/g). In contrast, HFA-CER displays no metastability and exhibits a reversible transition at ~68°C (ΔH = 7.3 cal/g). Interestingly, Pascher and coworkers (10–12) have suggested that the

Abbreviations: DSC, differential scanning calorimetry; C16:0-GalCer, d-erythro-N-palmitoyl-galactosyl-C_{18}-sphingosine; C16:0-GluCer, d-erythro-N-palmitoyl-glucosyl-C_{18}-sphingosine; GSL, glycosphingolipids; sulfatide, sulfated galactocerebroside; HIV, human immunodeficiency virus.

[1] Present address: Department of Cancer Biology, Dana Farber Cancer Research Institute and Harvard Medical School, Boston, MA 02115.

[2] To whom correspondence should be addressed.

function of 2-hydroxy fatty acids in GSL is to increase lateral interactions in the bilayer plane via hydrogen bonding, thus imparting greater bilayer stability.

The properties of galactocerebrosides and their interactions with other membrane lipids (particularly phosphatidylcholine and cholesterol) have been extensively studied (13–27). Our own studies have focused on partially synthetic d-erythro galactocerebrosides containing specific fatty acids of different chain length and chain unsaturation. For example, DSC and X-ray diffraction studies of partially synthetic N-palmitoyl-galactocerebroside also showed evidence of interconversions between metastable and stable bilayer phases, in this case thought to be accompanied by cerebroside hydration, prior to its high temperature, high enthalpy chain-melting transition (82°C, ΔH = 17.5 Kcal/mol) to a bilayer L_α phase (15). The hydrated stable form is stabilized by both a highly ordered chain-packing mode and a lateral intermolecular hydrogen bonding network involving the sphingosine backbone, the galactosyl group, and interbilayer water molecules (15). Similar bilayer phases and polymorphic transitions were observed for the longer chain homologues, C18:0- and C24:0-galactocerebroside (20, 24). However, some kinetic and structural differences were observed for C24:0-galactocerebroside presumably due to chain length differences of the fatty acid (C24) and sphingosine (C18) moieties (20). For C18-galactocerebrosides, increasing chain *cis*-unsaturation causes a progressive decrease in both the chain-melting transition temperature and its associated enthalpy (24). A similar effect of chain unsaturation was observed for C16-galactocerebrosides (28).

The properties of partially synthetic glucocerebrosides (29), as well as glucocerebrosides isolated both from the spleen of a patient with Gaucher's disease (29) and from rye leaves (30) have been studied by DSC and X-ray diffraction techniques. The calorimetric investigation of hydrated, partially synthetic C16:0-glucocerebroside showed an exothermic transition at 51°C, a weak endothermic transition at 65°C, followed by a high temperature (87.5°C), high enthalpy (17.1 kcal/mol) chain-melting transition (29). A similar pattern of exothermic/endothermic transitions, albeit at slightly lower temperatures (47 and 83°C), was observed for the Gaucher's glucocerebroside which contains predominantly long-chain saturated fatty acids (mainly C22:0 and C24:0). Using deuterium NMR, Skarjune and Oldfield (31) showed that the polar sugar head group of glucocerebroside extends away from the bilayer to allow maximum interaction with the bulk water layer. Rye glucocerebrosides, which contain predominantly (>95%) hydroxy fatty acids also show complex thermotropic phase behavior (30).

Naturally occurring cerebrosides, both GalCer and GluCer, are heterogeneous with respect to both their sphingosine component (chain length and Δ4–5 *trans* unsaturation) and their N-linked fatty acid chain (chain length, usually saturated long chain fatty acids, and hydroxylation). These cerebrosides show complex polymorphic phase behavior but it was thought that this complexity could in part, at least, derive from their structural heterogeneity. However, studies of chain-specific GalCer and GluCer (synthesized by deacylation and reacylation of naturally occurring cerebrosides) also showed a similar pattern of exothermic and endothermic transitions illustrative of polymorphic behavior (15, 29). The chain-melting transition of the saturated chain C16:0-, C18:0-, and C24:0-GalCer and C16:0-GluCer occurs at unusually high temperatures (>80°C) and exhibits large transition enthalpies (17–18 Kcal/mol) compared to other membrane lipids (e.g., phospholipids). A similar pattern of behavior has also been reported for partially synthetic sulfatides, i.e., sulfated galactocerebrosides (32–35).

With the availability of de novo synthetic protocols for sphingosine-specific and chain-specific d-erythro cerebrosides (36–40), we now present a comparative study of the structure and properties of the C16:0 fatty acyl versions of totally synthetic d-erythro GalCer and GluCer containing the specific C18:1 (*trans* Δ4–5) sphingosine base; the two sugars, d-galactose and d-glucose, differ only in the stereochemistry of the hydroxyl group at C4 of the sugar ring. A similar study of the two-sugar, lactosyl cerebroside also obtained by de novo synthetic methods will be reported separately (K. Saxena, P. Zimmermann, R. R. Schmidt, and G. G. Shipley, unpublished results).

MATERIALS AND METHODS

Cerebrosides

Totally synthetic *N*-palmitoyl-galactosyl-d-erythro-sphingosine (C16:0-GluCer) and *N*-palmitoyl-glucosyl-d-erythro-sphingosine (C16:0-GalCer) were synthesized starting from d-galactose as described previously (36–40).

Differential scanning calorimetry

Aliquots (1–4 mg) of C16:0-GalCer or C16:0-GluCer were transferred directly into preweighed stainless steel DSC pans. Doubly distilled water was added to the pans from a microsyringe to achieve the required hydration. Heating and cooling scans over the temperature range 0–100°C were performed either on a Perkin-Elmer (Norwalk, CT) DSC-2 or DSC-7 calorimeter. Heating and cooling rates ranged from 0.1 to 40°C. Peak maxima (or minima) were taken as the transition temperatures. The transition enthalpy was determined from the area under the transition peak by comparison with that of a known standard, gallium.

X-ray diffraction

Hydrated samples for X-ray diffraction were prepared by weighing anhydrous C16:0-GalCer or C16:0-GluCer into thin-walled capillary tubes (internal diameter 1 mm) followed by gravimetric addition of distilled deionized water. Samples were covered with parafilm, centrifuged at room temperature for about 2 min, and then flame-sealed. Equilibrated homogeneous dispersions were prepared by a cycle of centrifugation–sample inversion–centrifugation at a temperature above the previously determined transition temperature. Nickel-filtered CuK_α X-radiation from an Elliot GX-6 rotating anode generator (Elliot Automation, Borehamwood, U.K.) was focused by a toroidal mirror camera. X-ray diffraction patterns were recorded on photographic film and diffracted intensities were measured using a scanning microdensitometer (Joyce-Loebl, Gateshead, U.K.). The sample temperature was maintained (±1°C) with an automatically controlled ethylene glycol/water circulating bath.

RESULTS

Hydrated synthetic C16:0-GalCer

Differential scanning calorimetry. The calorimetric behavior of fully hydrated (70 wt % water) C16:0-GalCer is shown in **Fig. 1**. The initial heating scan (heating rate, 5°C/min) after sample equilibration by heating and cooling several times above and below the main, chain-melting transition temperature (see below) is shown in Fig. 1a. Hydrated C16:0-GalCer undergoes a broad (54–64°C), low-enthalpy exothermic transition centered at 59°C. Further heating results in the high temperature, high enthalpy endothermic transition at 85°C (ΔH = 17.9 kcal/mol C16:0-GalCer) characteristic of chain melting. Upon cooling from 90°C, hydrated C16:0-GalCer exhibits significant hysteresis or supercooling; a sharp exotherm is observed at 62°C followed by a lower enthalpy exotherm at 56°C (Fig. 1b). The total enthalpy under this complex exotherm is 8.6 kcal/mol. After cooling to 20°C, immediate re-heating results in a heating scan identical to that shown in Fig. 1a.

The nature of the exothermic transition at 59°C of C16:0-GalCer observed in the heating scan (Fig. 1a) was further investigated. The occurrence of this exothermic transition is dependent upon whether the sample is heated beyond or below the chain-melting transition temperature (**Fig. 2**). After initial heating and cooling scans (Figs. 2a and 2b), when hydrated C16:0-GalCer is heated to 70°C (i.e., below the 85°C transition), the exothermic transition at 59°C is present (Fig. 2c). On cooling, no transition is observed over the temperature range 70–30°C (Fig. 2d). Upon immediate reheating, the broad exothermic transition at 59°C does not reappear (Fig. 2e); however, the 85°C chain-melting transition is present with an enthalpy identical to that observed initially (see Figs. 2e and 2a). Subsequent cooling (Fig. 2f) and reheating to 90°C (data not shown) show behavior identical to that shown in Figs. 2b and 2a, respectively. These calorimetric data provide strong evidence for the presence of a metastable state, the conversion of which to a more stable state is accompanied

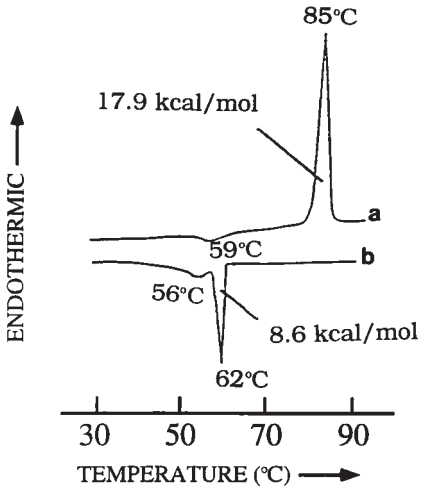

Fig. 1. DSC of hydrated (70 wt %) C16:0-GalCer. (a) Initial heating scan, 5°C/min; (b) cooling scan, 5°C/min.

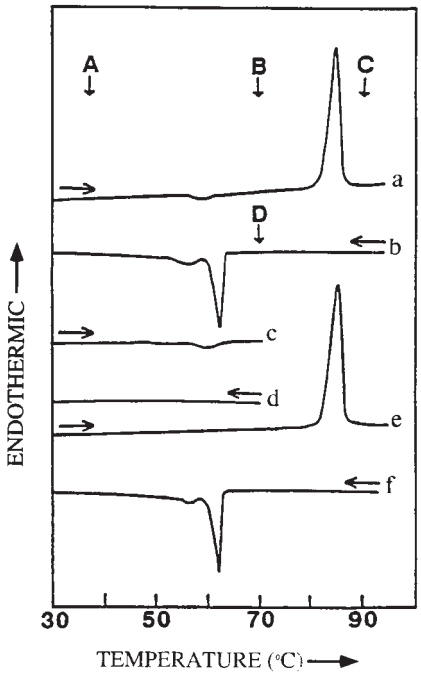

Fig. 2. DSC of hydrated (70 wt %) C16:0-GalCer. (a) Initial heating scan; (b) immediate cooling scan; (c) subsequent heating scan to 70°C immediately following cooling scan (b); (d) cooling scan from 70°C; (e) and (f) subsequent heating and cooling scans, respectively. Heating/cooling rates; 5°C/min. Lettered arrows indicate temperatures at which X-ray diffraction experiments were performed (see Fig. 4).

by the exothermic transition observed in the heating scans. Thus, the exothermic transition is irreversible in nature, its occurrence requiring prior heating above the chain-melting transition temperature.

The behavior of the exothermic transition in the heating scans was also studied as a function of prior cooling rate (**Fig. 3**). Hydrated C16:0-GalCer was cooled at various cooling rates and immediate heating scans at 5°C/min were recorded. Fig. 3A shows the behavior of exothermic transition in the heating scans. At prior fast cooling rates, 360 to 5°C/min, a broad exotherm is observed in the heating scans recorded immediately (Fig. 3A, scans a–f). However, at slow cooling rates ($\leq$2.5°C/min), no exotherm is observed in the subsequent heating scans (Fig. 3A, scans g and h). Thus, when C16:0-GalCer is cooled from melted-chain state at a very slow rate, there is sufficient time to permit the kinetically slow process of nucleation and growth of the stable form to occur. Apparently, the slowest cooling rates permit complete conversion to the stable form and no exothermic transition is observed in the heating scan (Figs. 3A, scans g and h). At the faster cooling rates, C16:0-GalCer crystallizes into the metastable form but insufficient time exists for the complete conversion of the metastable to the stable state. Therefore, in the next heating scan an exotherm (indicating the conversion of the metastable to stable form) is seen; the faster the prior cooling rate the less conversion to the stable form. The residual metastable form is subsequently converted to the stable form at 59°C on subsequent heating (Fig. 3A,

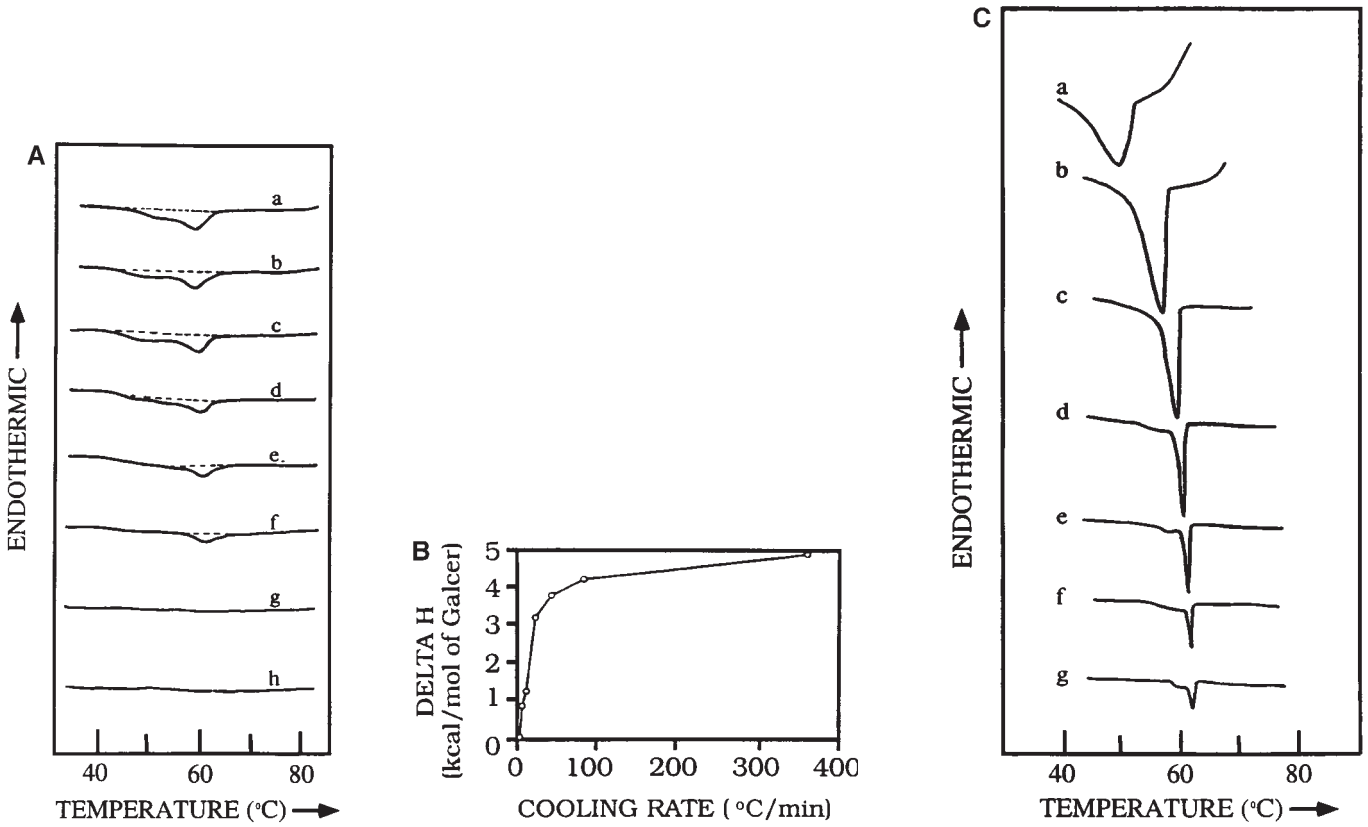

Fig. 3. (A) DSC of hydrated (70 wt %) C16:0-GalCer. Heating scans at 5°C/min showing the exotherm at 59°C immediately after cooling at different cooling rates; (a) 360, (b) 80, (c) 40, (d) 20, (e) 10, (f) 5, (g) 2.5, and (h) 1.25°C /min. (B) Effect of cooling rate on the enthalpy of the exothermic transition of hydrated (70 wt %) C16:0-GalCer. (C) DSC cooling scans of hydrated (70 wt %) C16:0-GalCer as a function of cooling rate; (a) 80, (b) 40, (c) 20, (d) 10, (e) 5, (f) 2.5, and (g) 1.25°C/min

scans f–a). The relationship between the exothermic enthalpy of the heating scan and the prior cooling rate is illustrated in Fig. 3B. The transition enthalpy increases with increasing cooling rate, the maximum enthalpy (4.9 kcal/mol C16:0-GalCer) being observed when the sample is quenched at 360°C/min from 90 to 30°C.

The complexity of the cooling curves at various cooling rates is depicted in Fig. 3C. At cooling rates 10°C/min or faster, only a single exotherm is observed. At slower cooling rates, this exotherm is resolved into a sharp peak with a small shoulder on the lower temperature side. An obvious explanation for the two-peak exotherm at slower cooling rates would be the initial formation of the metastable form from the melted-chain L_α phase (sharp peak in Fig. 3C, scans d–g), followed by a slow conversion of the metastable form into the stable form (low temperature shoulder in Fig. 3C, scans d–g). Although not obvious from the unscaled data shown in Fig. 3C, the maximum enthalpy associated with the two cooling exotherms (12.5 kcal/mol C16:0-GalCer) is observed at the slowest cooling rate (1.25°C/min). At faster cooling rates (>20°C/min), the enthalpy of the cooling exotherms becomes more or less constant (approx. 6.5 kcal/mol). We have also observed that low temperature incubation (−20°C) for prolonged periods of time results in the disappearance of the exothermic transition in the next heating scan; presumably, low temperature incubation also allows the slow conversion of any residual metastable form C16:0-GalCer into its stable form (data not shown).

X-ray diffraction. To elucidate the structural changes associated with the different transitions of hydrated C16:0-GalCer, X-ray diffraction patterns were recorded at different temperatures (see lettered arrows in Fig. 2). The diffraction pattern at 20°C shows six low-angle reflections indexing on a lamellar geometry corresponding to a bilayer periodicity, d = 56.7 Å (**Fig. 4A**). The wide angle region is characterized by a sharp reflection at $1/4.5$ Å^{-1}, a slightly broader reflection at $1/3.9$ Å^{-1}, and a very weak reflection at $1/5.0$ Å^{-1}.

When hydrated C16:0-GalCer, is heated to 70°C (above the exothermic transition, but below the high enthalpy endothermic transition), the diffraction pattern shown in Fig. 4B is observed. Eleven lamellar reflections are observed in the low angle region corresponding to a bilayer periodicity, d = 55.2 Å. Several sharp reflections are observed in the wide angle region, the most prominent of which are at $1/4.2$ Å^{-1} and $1/4.7$ Å^{-1}. This diffraction pattern is indicative of a highly ordered bilayer phase with crystalline hydrocarbon chain packing. On cooling to 20°C, the diffraction pattern recorded at this temperature (data not shown) is identical to that observed at 70°C (Fig. 4B). As expected (see Fig. 2), heating C16:0-GalCer back

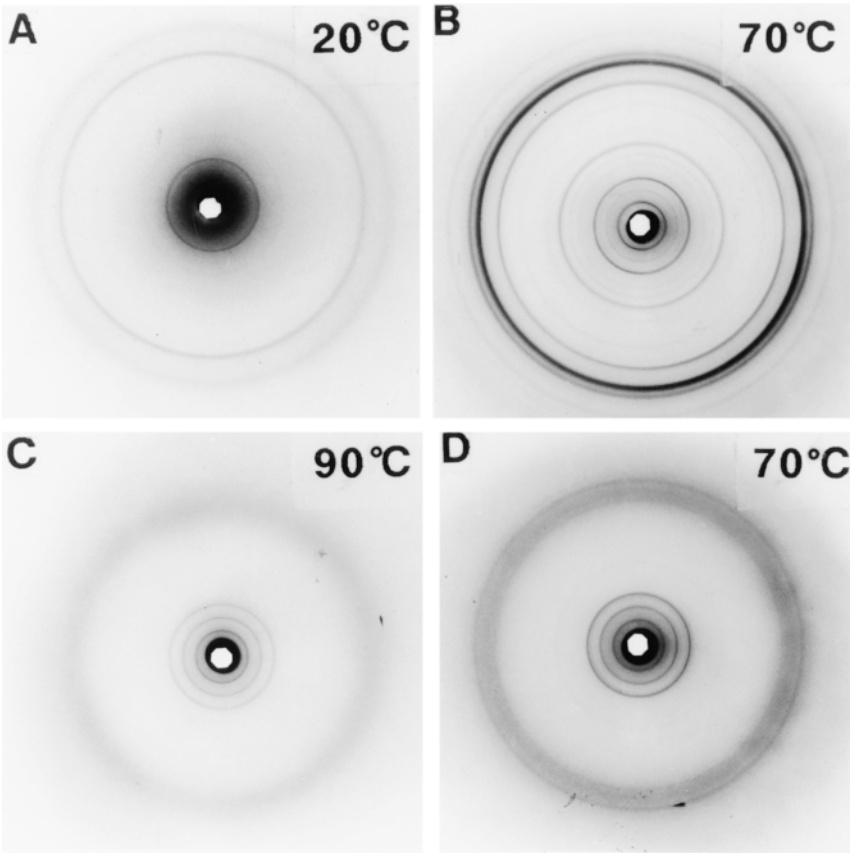

Fig. 4. X-ray diffraction patterns of hydrated (70 wt %) C16:0-GalCer recorded at different temperatures. (A) 20°C, metastable form, (B) 70°C, stable form, (C) 90°C, liquid–crystalline form, and (D) 70°C after cooling from 90°C; coexisting phases.

to 70°C leads to no change in the diffraction pattern (data not shown). Upon further heating to 90°C, i.e., beyond the 85°C endothermic transition, a diffraction pattern characteristic of a liquid–crystalline bilayer phase is observed (Fig. 4C). The low angle region shows four lamellar reflections corresponding to a bilayer periodicity, d = 50.2 Å. A broad, diffuse reflection centered at 1/4.6 $Å^{-1}$ characteristic of the disordered hydrocarbon chain packing in the melted-chain state is observed. Thus, above the chain-melting transition hydrated C16:0-GalCer forms a bilayer L_α phase.

After cooling from 90 to 70°C, hydrated C16:0-GalCer gives a diffraction pattern (Fig. 4D) characteristic of coexisting bilayer phases, the L_α phase and the stable crystalline phase. The wide-angle region shows two sharp reflections at 1/4.7 $Å^{-1}$ and 1/4.2 $Å^{-1}$, as well as a broad and not clearly defined reflection at approx. 1/4.6 $Å^{-1}$ indicative of the presence of the L_α phase. Further cooling to 20°C results in a diffraction pattern (not shown) similar to that of the stable crystalline form (see Fig. 4B). Presumably the slow cooling rate in the X-ray sample holder and the 2- to 5-h exposure time is sufficient to allow conversion of the initially formed metastable phase to the stable crystalline bilayer phase.

The diffraction pattern of anhydrous C16:0-GalCer (data not shown) is very similar to that of hydrated C16:0-GalCer at 20°C (see Fig. 4A). The low-angle region shows three reflections corresponding to a bilayer periodicity, d = 56.2 Å; two wide-angle reflections at 1/4.5 and 1/3.8 $Å^{-1}$ are observed.

Hydrated synthetic C16:0-GluCer

Differential scanning calorimetry. The thermotropic behavior of hydrated C16:0-GluCer is similar to that of hydrated C16:0-GalCer. The first heating scan (5°C/min) after equilibration shows two transitions, a broad (range 44–56°C), low enthalpy (ΔH = 1.4 kcal/mol) exothermic transition at 48°C followed by a high enthalpy (ΔH = 14.9 kcal/mol) endothermic transition at 87°C (**Fig. 5a**). Upon cooling from 95°C, two overlapping exothermic transitions are observed at 67 and 61°C (Fig. 5b). The total enthalpy associated with the two exotherms is 10.2 kcal/mol.

As with hydrated C16:0-GalCer, the occurrence of the exothermic transition of C16:0-GluCer in the heating run is dependent on whether the sample has been heated beyond the chain-melting transition (**Fig. 6**). The initial heating and cooling scans (Fig. 6, a and b) are identical to those described above (Fig. 5). The next heating scan to 70°C (Fig. 6c) shows the exotherm at 48°C; however, on cooling from 70 to 0°C, no exothermic transitions are observed (compare Figs. 6d and 6b). The subsequent heating scan (Fig. 6e) shows no evidence of the 48°C exotherm, only

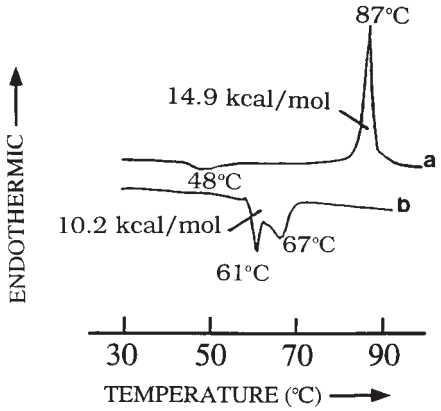

Fig. 5. DSC of hydrated (70 wt %) C16:0-GluCer. (a) Initial heating scan, 5°C/min; (b) cooling scan, 5°C/min.

the high enthalpy chain-melting transition at 87°C is observed. Subsequent cooling (Fig. 6f) and heating (Fig. 6g) scans are identical to those recorded previously (Fig. 6, b and a, respectively). Thus, once the stable phase has been formed, reappearance of the metastable form requires conversion to the melted chain phase and subsequent cooling.

To probe further the behavior of the 48°C exotherm, heating scans (5°C/min) were recorded immediately after cooling at different cooling rates (**Fig. 7A**). After prior cooling at rates ≤1.25°C/min (Fig. 7A, scans f and g), no detectable exothermic transition at 48°C was observed in the heating scan. At faster prior cooling rates the exotherm at 48°C is present (Fig. 7A, scans a–e). In addition, the enthalpy of the endothermic, chain-melting transition at 87°C is independent of the previous cooling rate (Fig. 7A). The cooling scans themselves are shown in Fig. 7B. At cooling rates ≥10°C/min only a single exothermic transition is observed upon cooling (Fig. 7B, scans a–c). At slower cooling rates two exotherms are observed. However, unlike the cooling exotherms of hydrated C16:0-GalCer in which the shoulder appears on the low temperature side of the exotherm, for C16:0-GluCer the shoulder appears on the high temperature side (compare Figs. 7B and 3C). The total enthalpy of the cooling exotherm(s) increases with a decrease in the cooling rate (Fig. 7C). At the slowest cooling rate (0.63°C/min), the exothermic enthalpy (14.5 kcal/mol C16:0-GluCer) is essentially identical to that of the endothermic chain-melting transition observed on heating (14.9 kcal/mol).

Although overnight incubation at 0°C does not result in the disappearance of the exothermic transition, after prolonged (180 h), low-temperature (−20°C) storage of C16:0-GluCer, no exothermic transition is observed in the initial heating scan, only the chain-melting transition at 87°C occurs (data not shown). Thus, slow conversion of the metastable form to the stable form does occur as a consequence of long term, low temperature equilibration.

X-ray diffraction. X-ray diffraction patterns of hydrated C16:0-GluCer were recorded at different temperatures (see lettered arrows in Fig. 6). The diffraction pattern at

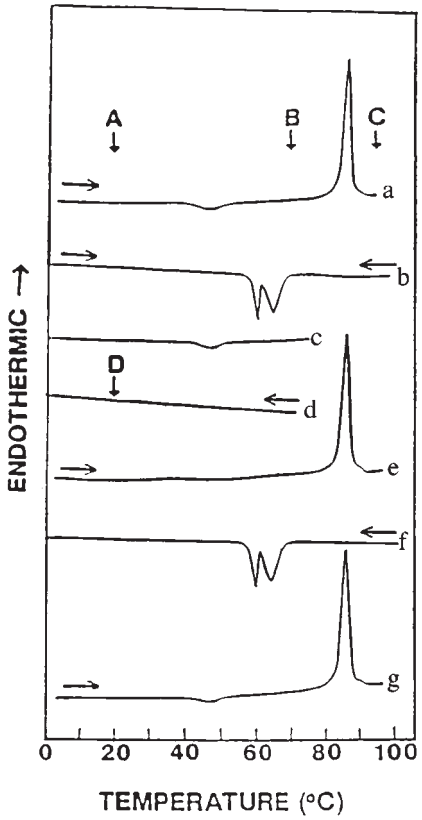

Fig. 6. DSC of hydrated (70 wt %) C16:0-GluCer. (a) Initial heating scan; (b) immediate cooling scan; (c) subsequent heating scan to 70°C immediately following cooling scan (b); (d) cooling scan from 70°C; (d), (e) and (f) subsequent heating, cooling and reheating scans, respectively. Heating/cooling rates; 5°C /min. Lettered arrows indicate temperatures at which X-ray diffraction experiments were performed (see Fig. 8).

20°C (**Fig. 8A**) was recorded after the sample was equilibrated by temperature cycling above and below the chain-melting transition (87°C). The low-angle reflections index according to a bilayer periodicity, d = 52.3Å. Several reflections are observed in the wide-angle region, the most prominent occurring at 1/4.5, 1/4.2, and 1/3.7 $Å^{-1}$.

Heating to 70°C, beyond the exothermic transition, results in changes in the diffraction pattern as shown in Fig. 8B. A series of lamellar reflections correspond to a bilayer periodicity, d = 53.9Å is observed. Again, several reflections are observed in the wide-angle region, the strongest being at 1/4.44 and 1/4.14 $Å^{-1}$; weaker reflections at 1/5.6 and 1/5.0 $Å^{-1}$ are also observed.

After cooling to 20°C, a diffraction pattern (data not shown) essentially identical to that shown in Fig. 8B is obtained. In the wide-angle region, the two most prominent reflections occur at 1/4.43 and 1/4.06 $Å^{-1}$, with a weaker reflection at 1/3.9 $Å^{-1}$. The small differences in the wide-angle reflections at the two temperatures (70 and 20°C) are probably due to temperature-induced lattice expansion/contraction effects.

The X-ray diffraction pattern of hydrated C16:0-GluCer recorded at 95°C, above the chain-melting transition, is shown in Fig. 8C. Four lamellar reflections corresponding

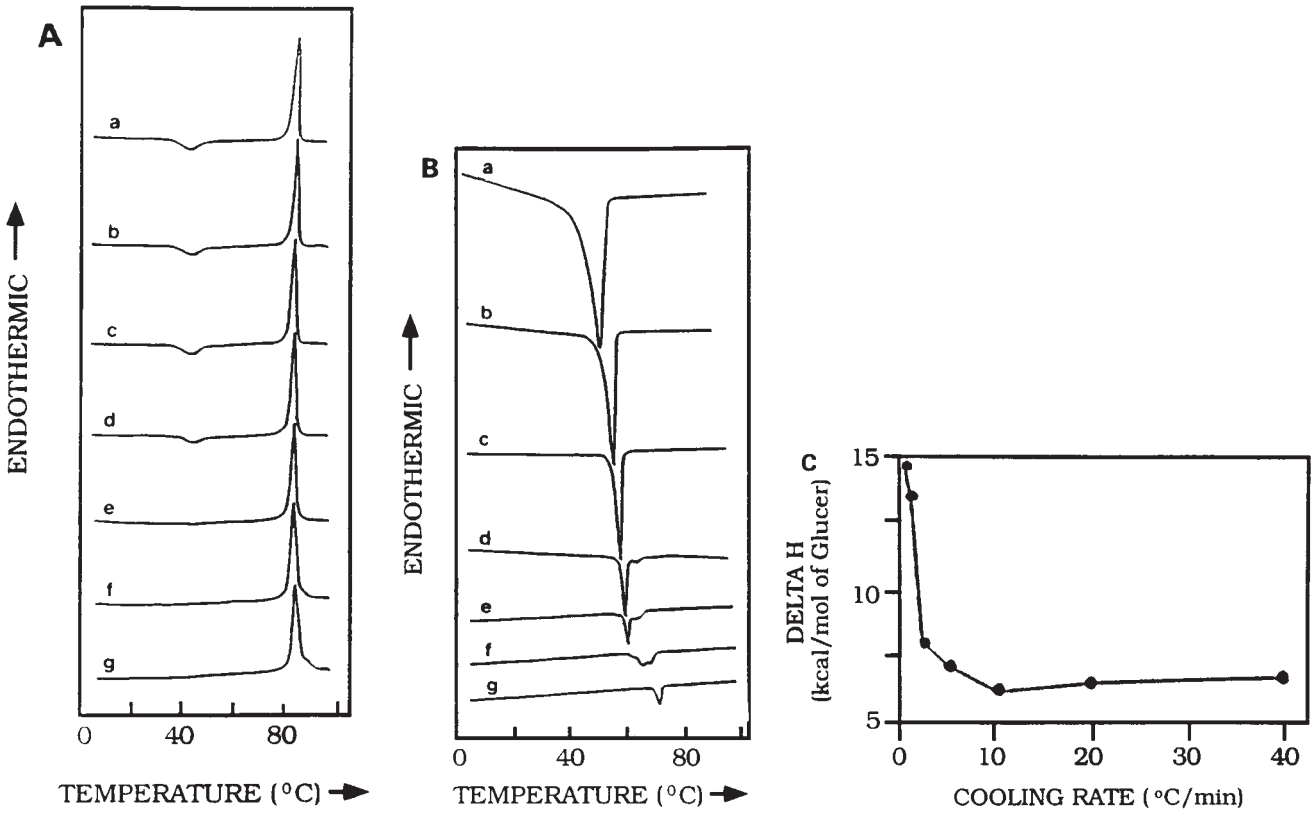

Fig. 7. (A) DSC of hydrated (70 wt %) C16:0-GluCer. Heating scans at 5°C / min showing the exotherm at 48°C immediately after cooling at different cooling rates; (a) 40, (b) 20, (c) 10, (d) 5, (e) 2.5, (f) 1.25, and (g) 0.63°C / min. (B) DSC cooling scans of hydrated (70 wt %) C16:0-GluCer as a function of cooling rate; (a) 40, (b) 20, (c) 10, (d) 5, (e) 2.5, (f) 1.25, and (g) 0.63°C / min. (C) Transition enthalpy of the complex exothermic transition as a function of cooling rate.

to a bilayer periodicity, d = 50.8 Å are observed in the low-angle region. The diffuse broad wide-angle reflection at 1/4.6 $Å^{-1}$ confirms the presence of the melted chain L_α bilayer phase. On cooling to 20°C, a diffraction pattern (Fig. 8D) similar to that of the stable phase (Fig. 8C) is observed. Again, the long X-ray exposure time presumably permits extensive conversion to the stable phase.

DISCUSSION

While the physical properties of isolated and partially synthetic galacto- and gluco-cerebrosides have been the subject of several investigations, the availability of totally synthetic cerebrosides (chemically pure with respect to stereochemistry, fatty acid, and sphingosine composition) and other more complex GSL offers the opportunity for further studies. Here, we have compared the behavior of synthetic C16:0 galacto- and gluco-cerebrosides at full hydration. The DSC data clearly show that the thermotropic properties of the two cerebrosides are quite similar. After equilibration by temperature cycling about the chain-melting transition, both cerebrosides show a low temperature exothermic transition and a high temperature, high enthalpy endothermic transition (Figs. 1 and 5). The high temperature transitions occur at 85 and 87°C for C16:0-GalCer and C16:0-GluCer, respectively, although the transition enthalpy for the glucosyl compound is significantly smaller (14.9 versus 17.9 kcal / mol). The X-ray diffraction data (Figs. 4 and 8) confirm that in both cases this high temperature, high enthalpy transition is due to hydrocarbon chain melting. More specifically, a stable bilayer phase with the fatty acyl and sphingosyl chains arranged in a highly ordered crystalline packing mode (Figs. 4B and 8B) converts to liquid crystalline bilayer phase, L_α, with melted hydrocarbon chains (Figs. 4C and 8C). For both cerebrosides, chain melting is accompanied by a decrease in bilayer periodicity (3–5 Å). The bilayer periodicities in the L_α phase are essentially identical, 50.2 and 50.8Å, suggesting that, in this phase at least, the isomeric form of the hexose, galactose or glucose, is not a significant determinant of bilayer structure, bilayer hydration, or interbilayer attractive or repulsive forces.

In contrast to the chain-melting transitions, the low enthalpy exotherms on heating occur at significantly different temperatures, 59°C for C16:0-GalCer and 48°C for C16:0-GluCer (Figs. 1 and 5). We have confirmed that in both cases this transition is irreversible (Figs. 2 and 6). Cooling from a temperature intermediate between the exotherm and the chain-melting transition (e.g., 70°C) shows no exotherm on either the cooling or next heating scan. Under these conditions, the bilayer phase present is stable from 0°C (and probably lower) up to the respective

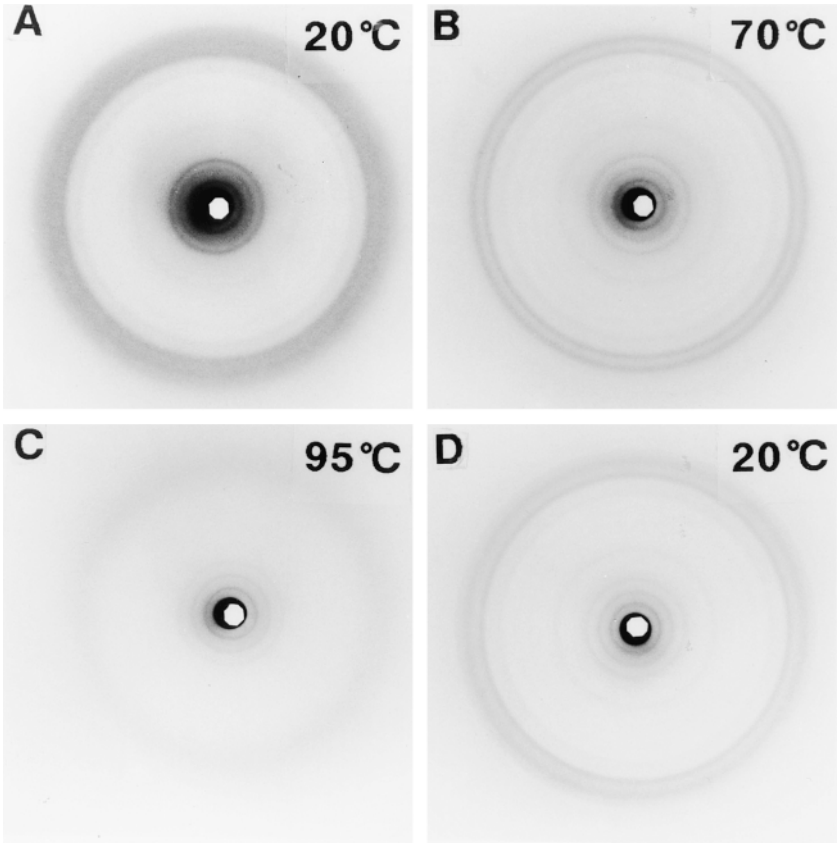

Fig. 8. X-ray diffraction patterns of hydrated (70 wt %) C16:0-GluCer recorded at different temperatures. (A) 20°C, metastable form, (B) 70°C, stable form, (C) 95°C, liquid–crystalline form, and (D) 20°C after cooling from 95°C; coexisting phases.

chain-melting temperature (85 or 87°C). Clearly, the exothermic transition represents the conversion of a metastable phase to a stable phase. For both C16:0-GalCer and C16:0-GluCer the X-ray diffraction data show convincingly that both the metastable and stable phases have bilayer packing arrangements (Fig. 4, A and B; Fig. 6, A and B). The bilayer periodicities of the stable phase of C16:0-GalCer and C16:0-GluCer are quite similar 54–55Å, and the wide-angle reflections argue for ordered chain packing arrangements for the two cerebrosides (Figs. 4B and 8B). Thus, the stable bilayer phases of C16:0-GalCer and C16:0-GluCer appear to be quite similar and, as evidenced by the numerous wide-angle reflections, both adopt a highly ordered "crystalline" chain-packing arrangement. In contrast, the structures of the metastable phases appear to differ somewhat. Notably, the bilayer periodicity of C16:0-GluCer is approximately 5Å less than that of its galactosyl counterpart (Figs. 4A and 8A) and in addition, the wide-angle patterns differ, suggesting differences in the chain-packing modes for the two cerebrosides (Figs. 4A and 8A). However, the X-ray diffraction patterns of both "hydrated" C16:0-GalCer and C16:0-GluCer in the metastable state strongly resemble those of the corresponding anhydrous forms (data not shown). This observation leads to the conclusion that on cooling from the melted-chain bilayer L_α phase, both chain crystallization and cerebroside dehydration occur initially. Presumably the slow conversion to the stable phase requires both rehydration of the polar interface, as well as modifications to the chain packing.

The cooling data for C16:0-GalCer and C16:0-GluCer shown in Figs. 3 and 7, respectively, provide kinetic data relevant to the stepwise (presumably) conversion of the melted-chain L_α bilayer phase to the metastable bilayer phase, followed by conversion to the stable bilayer phase. First, it is clear that even at the slowest cooling rate a significant supercooling effect ($\geqslant$15°C) exists for both cerebrosides before chain "crystallization" occurs (Fig. 3C, scan g; Fig. 7B, scan g). For C16:0-GalCer it would appear that at the faster cooling rates conversion to the metastable phase occurs (major peak in Fig. 3C), whereas relatively little of the stable phase can form. Note that on the subsequent heating scan, exothermic conversion to the stable phase at 59°C occurs extensively, the maximum enthalpy for this transition being observed after the fastest cooling rate (see Fig. 3, A and B). Similar, but not identical (see below), behavior is observed for C16:0-GluCer (Fig. 7, A and B).

For both cerebrosides at very slow cooling rates, exothermic conversion to the stable phase is kinetically permitted and complete conversion to the stable form occurs prior to the next heating scan where no exothermic transition is ob-

served (Fig. 3A, scans g and h; Fig. 7A, scans f and g). In addition, for C16:0-GluCer at the slowest cooling rate, the enthalpy associated with the cooling exotherms is essentially identical to that of the chain-melting transition on heating (Fig. 7C); similar observations have been made for C16:0-GalCer (data not shown). At intermediate cooling rates (e.g., 5°C/min), two transitions are observed. For C16:0-GalCer the upper transition would appear to correspond to conversion to the metastable phase; the lower transition (a shoulder in Fig. 3C), increasing in enthalpy with decreasing cooling rate, presumably reflects formation of the stable phase. The reverse appears to be true for C16:0-GluCer, with the *high temperature* shoulder becoming more pronounced at slower cooling rates, eventually becoming a single, high enthalpy (15 kcal/mol) transition (Fig. 7, B and C). For C16:0-GalCer a stepwise pathway may occur, i.e., initial formation of the metastable phase at the higher temperature exotherm followed by exothermic conversion, at least partially, to the stable form at the lower temperature exotherm. Complete conversion occurs either via the exothermic transition on subsequent heating or as a result of low temperature incubation. C16:0-GluCer, on the other hand, appears to form the stable phase at the higher temperature exotherm, with conversion of any residual L_α phase to the metastable phase at the lower temperature exotherm. As for C16:0-GalCer, conversion of the metastable phase of C16:0-GluCer to the stable phase occurs exothermically either via the exothermic transition on subsequent heating or as a result of low temperature incubation.

In terms of structure, C16:0-GalCer and C16:0-GluCer exhibit essentially identical structures in both their L_α and stable bilayer phases (see above). While their metastable bilayer phases differ somewhat in both bilayer periodicity and chain packing, both appear to have an ordered, "crystalline" chain packing arrangement rather than the hexagonal chain packing characteristic of bilayer gel phases of, for example, phospholipids. Thus, the exotherm observed on heating represents a metastable–stable transition accompanied by *i*) a change in the chain packing mode, and *ii*) bilayer hydration. The stable bilayer phase formed also has a highly ordered, but different, "crystalline" chain packing mode. The stable "crystalline-chain", bilayer phases of both C16:0-GalCer and C16:0-GluCer undergo a chain-melting transition to their bilayer L_α phases with a significantly higher enthalpy (15–18 kcal/mol) than observed in bilayer gel–bilayer L_α transitions of most phospholipids (approx. 7 kcal/mol). A summary comparing the bilayer parameters of the three phases (metastable (A), stable (B), and liquid crystal (C)) of C16:0-GalCer and C16:0-GluCer is shown in **Fig. 9**.

It is worth noting that in extensive studies of synthetic glyco-glycerolipids, Hinz and colleagues (41–44) and, more recently, McElhaney and colleagues (45–50) also find that synthetic galacto- and glucoglycerolipids exhibit structural and thermodynamic properties similar to the cerebrosides. For example, at "low" temperatures, these glycoglycerolipids exhibit conversions between metastable and stable bilayer phases, a behavior similar to that of

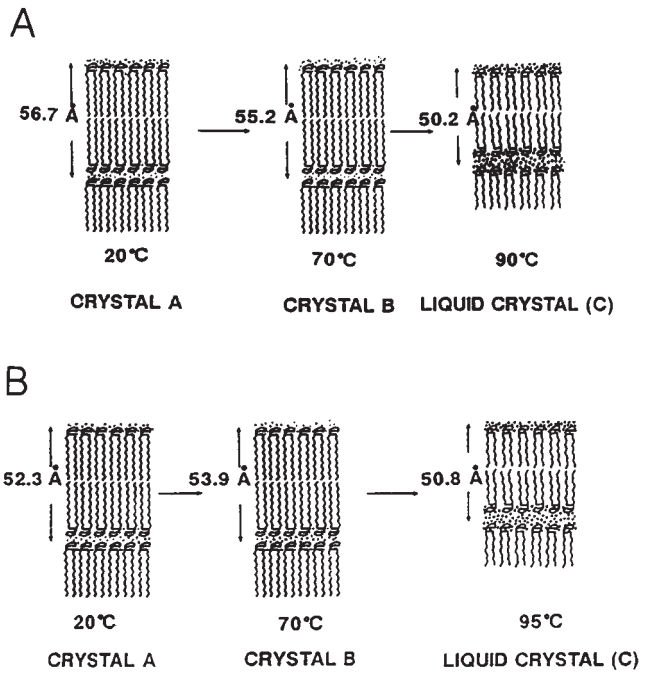

Fig. 9. Schematic representation of the temperature-dependent structural changes of (A) C16:0-GalCer, and (B) C16:0-GluCer.

the cerebrosides described here. At temperatures above the chain-melting transition, these glycero-based lipids tend to form the L_α bilayer phase, but at higher temperatures they also form non-bilayer (hexagonal, cubic, etc.) phases. As the synthetic cerebrosides exhibit chain-melting transitions higher than 80°C we have been unable to demonstrate non-bilayer phase formation; the L_α phase appears to be stable at least up to 95°C. Although the sugar groups present in both the sphingosine-based and glycerol-based glycolipids contribute to the thermotropic properties described above, we should point out that the low temperature polymorphic behavior of the two cerebrosides described here is essentially mimicked by the behavior of synthetic C16:0 d-erythro ceramide lacking a sugar moiety (51); for example, compare our Figs. 2 and 6 with Fig. 3 from Shah et al. (51). This suggests that, while interfacial hydrogen bonding interactions via the sugar residues remain important, changes in hydrocarbon chain packing presumably contribute significantly to the similar polymorphic effects observed for both ceramides and cerebrosides.

In summary, the two totally synthetic cerebrosides (C16:0-GalCer and C16:0-GluCer) examined in this paper show complex thermal behavior with interconversions between metastable and stable bilayer "crystalline" chain phases. However, it should be noted that the behavior of the two totally synthetic cerebrosides described here is quite similar to that of the corresponding partially synthetic C16:0 cerebrosides described previously (15, 29). Thus, minor variations in the structure of the sphingosine chain (chain length, Δ4–5 unsaturation, etc.) appear to have relatively little effect on the thermotropic properties of these cerebrosides.

This research was supported by Research Grants HL-26335 and HL-57405, and Training Grant HL-07291 from the National Institutes of Health.

Manuscript received 12 October 1998 and in revised form 15 January 1999.

REFERENCES

1. Harouse, J. M., S. Bhat, S. L. Spitalnik, M. Laughlin, K. Stefano, D. H. Silberberg, and F. Gonzalez-Scarano. 1991. Inhibition of entry of HIV-1 in neural cell lines by antibodies against galactosyl ceramide. *Science*. **253:** 320–323.
2. van den Berg, L. H., S. A. Sadiq, S. Lederman, and N. Latov. 1992. The gp120 glycoprotein of HIV-1 binds to sulfatide and to myelin associated glycoprotein. *J. Neurosci. Res.* **33:** 513–518.
3. Fishman, P. H., T. Pacuszka, and P. A. Orlandi. 1993. Gangliosides as receptors for bacterial enterotoxins. *Adv. Lipid Res.* **25:** 165–187.
4. Reed, R. A., and G. G. Shipley. 1996. Properties of ganglioside G_{M1} in phosphatidylcholine bilayer membranes. *Biophys. J.* **70:** 1363–1372.
5. Reed, R. A., J. M. Mattai, and G. G. Shipley. 1987. Interaction of cholera toxin with ganglioside G_{M1} receptors in supported monolayers. *Biochemistry.* **26:** 824–832.
6. Zhang, R., M. L. Westbrook, E. M. Westbrook, D. L. Scott, Z. Otwinowski, P. R. Maulik, R. A. Reed, and G. G. Shipley. 1995. The 2.4Å crystal structure of cholera toxin B subunit pentamer: choleragenoid. *J. Mol. Biol.* **251:** 550–562.
7. Zhang, R., D. L. Scott, M. L. Westbrook, S. Nance, B. D. Spangler, G. G. Shipley, and E. M. Westbrook. 1995. The three-dimensional crystal structure of cholera toxin. *J. Mol. Biol.* **251:** 563–573.
8. Reiss-Husson, F. 1967. Structure of liquid-crystalline phases of different phospholipids, monoglycerides and sphingolipids in the absence and presence of water. *J. Mol. Biol.* **25:** 363–382.
9. Curatolo, W. 1982. Thermal behavior of fractionated and unfractionated bovine brain cerebrosides. *Biochemistry.* **21:** 1761–1764.
10. Pascher, I. 1976. Molecular arrangements in sphingolipids. Conformation and hydrogen bonding of ceramide and their implication on membrane stability and permeability. *Biochim. Biophys. Acta.* **455:** 433–451.
11. Lofgren, H., and I. Pascher. 1977. Molecular arrangements of sphingolipids. The monolayer behavior of ceramides. *Chem. Phys. Lipids.* **20:** 273–284.
12. Pascher, I., and S. Sundell. 1977. Molecular arrangement in sphingolipids. The crystal structure of cerebroside. *Chem. Phys. Lipids.* **20:** 175–191.
13. Bunow, M. R. 1979. Two gel states of cerebrosides: calorimetric and Raman spectroscopic evidence. *Biochim. Biophys. Acta.* **574:** 542–546.
14. Bunow, M. R., and I. W. Levin. 1980. Molecular conformations of cerebrosides in bilayers determined by Raman spectroscopy. *Biophys. J.* **32:** 1007–1021.
15. Ruocco, M. J., D. Atkinson, D. M. Small, R. P. Skarjune, E. Oldfield, and G. G. Shipley. 1981. X-ray diffraction and calorimetric study of anhydrous and hydrated N-palmitoylgalactosylsphingosine (cerebroside). *Biochemistry.* **21:** 5957–5966.
16. Ruocco, M. J., G. G. Shipley, and E. Oldfield. 1983. Galactocerebroside-phospholipid interactions in bilayer membranes. *Biophys. J.* **43:** 91–101.
17. Ruocco, M. J., and G. G. Shipley. 1983. Hydration of N-palmitoylgalactosylsphingosine compared to monosaccharide hydration. *Biochim. Biophys. Acta.* **735:** 305–308.
18. Ruocco, M. J., and G. G. Shipley. 1984. Interaction of cholesterol with galactocerebroside and galactocerebroside-phosphatidylcholine bilayer membranes. *Biophys. J.* **46:** 695–707.
19. Curatolo, W., and F. B. Jungalwala. 1985. Phase behavior of galactocerebrosides from bovine brain. *Biochemistry.* **24:** 6608–6613.
20. Reed, R. A., and G. G. Shipley. 1987. Structure and metastability of N-lignocerylgalactosylsphingosine (cerebroside) bilayers. *Biochim. Biophys. Acta.* **896:** 153–164.
21. Bunow, M. R., and I. W. Levin. 1988. Phase behavior of cerebroside and its fractions with phosphatidylcholines: calorimetric studies. *Biochim. Biophys. Acta.* **939:** 577–586.
22. Johnston, D. S., and D. Chapman. 1988. A calorimetric study of the thermotropic behaviour of mixtures of brain cerebrosides with other brain lipids. *Biochim. Biophys. Acta.* **939:** 603–614.
23. Jackson, M., D. S. Johnston, and D. Chapman. 1988. Differential scanning calorimetric and Fourier transform infrared spectroscopic investigations of cerebroside polymorphism. *Biochim. Biophys. Acta.* **944:** 497–506.
24. Reed, R. A., and G. G. Shipley. 1989. Effect of chain unsaturation on the structure and thermotropic properties of galactocerebrosides. *Biophys. J.* **55:** 281–292.
25. Ali, S., H. L. Brockman, and R. E. Brown. 1991. Structural determinants of miscibility in surface films of galactosylceramide and phosphatidylcholine: effect of unsaturation in the galactosylceramide acyl chain. *Biochemistry.* **30:** 11198–11205.
26. Ali, S., J. M. Smaby, and R. E. Brown. 1993. Acyl structure regulates galactosylceramide's interfacial interactions. *Biochemistry.* **32:** 11696–11703.
27. Ali, S., J. M. Smaby, H. L. Brockman, and R. E Brown. 1994. Cholesterol's interfacial interactions with galactosylceramides. *Biochemistry.* **33:** 2900–2906.
28. Haas, N. S., and G. G. Shipley. 1995. Structure and properties of N-palmitoleoyl-galactosylsphingosine (cerebroside). *Biochim. Biophys. Acta.* **1240:** 133–141.
29. Freire, E., D. Bach, M. Correa-Freire, I. Miller, and Y. Barenholz. 1980. Calorimetric investigation of the complex phase behavior of glucocerebroside dispersions. *Biochemistry.* **19:** 3662–3665.
30. Lynch, D. V., M. Caffrey, J. L. Hogan, and P. L. Steponkus. 1992. Calorimetric and X-ray diffraction studies of rye glucocerebroside. *Biophys. J.* **61:** 1289–1300.
31. Skarjune, R., and E. Oldfield. 1982. Physical studies of cell surface and cell membrane structure. Deuterium magnetic resonance studies of N-palmitoylglucosylceramide (cerebroside) head group structure. *Biochemistry.* **21:** 3154–3160.
32. Koshy, K. M., and J. M. Boggs. 1983. Partial synthesis and physical properties of cerebroside sulfate containing palmitic acid or alpha-hydroxy palmitic acid. *Chem. Phys. Lipids.* **34:** 41–53.
33. Boggs, J. M., K. M. Koshy, and G. Rangaraj. 1984. Effect of fatty acid chain length, fatty acid hydroxylation, and various cations on the behavior of synthetic cerebroside sulfate. *Chem. Phys. Lipids.* **36:** 65–89.
34. Boggs, J. M., K. M. Koshy, and G. Rangaraj. 1988. Influence of structural modifications on the phase behavior of semi-synthetic cerebroside sulfate. *Biochim. Biophys. Acta.* **938:** 361–372.
35. Boggs, J. M., K. M. Koshy, and G. Rangaraj. 1988. Interdigitated lipid bilayers of long acyl chain species of cerebroside sulfate. A fatty acid spin label study. *Biochim. Biophys. Acta.* **938:** 373–385.
36. Schmidt, R. R., and R. Klager. 1985. Short synthesis of cerebrosides. *Angew. Chem. Int. Ed. Engl.* **24:** 65–66.
37. Schmidt, R. R. 1986. New methods for the synthesis of glycosides and oligosaccharides. Are there alternatives to the Koenigs-Knorr method? *Angew. Chem. Int. Ed. Engl.* **25:** 212–235.
38. Schmidt, R. R., and P. Zimmermann. 1986. Synthesis of glycosphingolipids and psychosines. *Angew. Chem. Int. Ed. Engl.* **25:** 725–726.
39. Schmidt, R. R., and P. Zimmermann. 1986. Synthesis of d-erythro-sphingosines. *Tetrahedron Lett.* **27:** 481–484.
40. Zimmermann, P., R. Bommer, T. Bar, and R. R. Schmidt. 1988. Azidosphingosine glycosylation in glycosphingolipid synthesis. *J. Carbohydrate Chem.* **7:** 435–452.
41. Hinz, H-J., H. Kuttenreich, R. Meyer, M. Renner, R. Frund, R. Koynova, A. I. Boyanov, and B. G. Tenchov. 1991. Stereochemistry and size of sugar headgroups determine structure and phase behavior of glycolipid membranes: densitometric, calorimetric and X-ray studies. *Biochemistry.* **30:** 5125–5138.
42. Hinz, H-J., L. Six, K-P. Reuss, and M. Lieflander. 1985. Head-group contributions to bilayer stability: monolayer and calorimetric studies on synthetic, stereochemically uniform glucolipids. *Biochemistry.* **24:** 806–813.
43. Kuttenreich, H., H-J. Hinz, M. Inczedy-Marcsek, R. Koynova, B. Tenchov, and P. Laggner. 1988. Polymorphism of synthetic 1,2-dialkyl-3-O-β-d-galactosyl-*sn*-glycerols of different chain lengths. *Chem. Phys. Lipids.* **47:** 245–260.
44. Koynova, R. D., H. L. Kuttenreich, B. G. Tenchov, and H-J. Hinz. 1988. Influence of head-group interactions on the miscibility of synthetic stereochemically pure glycolipids and phospholipids. *Biochemistry.* **27:** 4612–4619.
45. Mannock, D. A., R. N. A. H. Lewis, A. Sen, and R. N. McElhaney. 1988. The physical properties of glycosyl diacylglycerols. Calorimetric studies of a homologous series of 1,2-di-O-acyl-3-O-(β-d-glucopyranosyl)-*sn*-glycerols. *Biochemistry.* **27:** 6852–6859.

46. Mannock, D. A., R. N. A. H. Lewis, and R. N. McElhaney. 1990. The physical properties of glycosyl diacylglycerols. 1. Calorimetric studies of a homologous series of 1,2-di-O-acyl-3-O-(α-d-glucopyranosyl)-*sn*-glycerols. *Biochemistry.* **29:** 7790–7799.
47. Mannock, D. A., R. N. McElhaney, P. E. Harper, and S. M. Gruner. 1994. Differential scanning calorimetry and x-ray diffraction studies the thermotropic phase behavior of the diastereomeric di-tetradecyl-β-d-galactosyl glycerols and their mixture. *Biophys. J.* **66:** 734–740.
48. Sen, A., S. Hui, D. A. Mannock, R. N. A. H. Lewis, and R. N. McElhaney. 1990. The physical properties of glycosyl diacylglycerols. 2. X-ray diffraction studies of a homologous series of 1,2-di-O-acyl-3-O-(α-d-glucopyranosyl)-*sn*-glycerols. *Biochemistry.* **29:** 7799–7804.
49. Lewis, R. N. A. H., D. A. Mannock, R. N. McElhaney, P. T. T. Wong, and H. H. Mantsch. 1990. Physical properties of glycosyldiacylglycerols. An infrared spectroscopic study of the gel phase polymorphism of 1,2-di-O-acyl-3-O-(β-d-glucopyranosyl)-*sn*-glycerols. *Biochemistry.* **29:** 8933–8943.
50. Mannock, D. A., and R. N. McElhaney. 1991. Differential scanning calorimetry and X-ray diffraction studies of a series of synthetic β-d-galactosyl diacyglycerols. *Biochem. Cell Biol.* **69:** 863–867.
51. Shah, J., J. M. Atienza, R. I. Duclos, A. V. Rawlings, Z. Dong, and G. G. Shipley. 1995. Structural and thermotropic properties of synthetic C16:0 (palmitoyl) ceramide: effect of hydration. *J. Lipid Res.* **36:** 1936–1944.